World Electric Vehicle Journal

Article

Optimized Synchronous SPWM Modulation Strategy for Traction Inverters Based on Non-Equally Spaced Carriers

Xuefeng Jin [1], Shiwei Li [1], Wenbo Sun [2], Wei Chen [1,*], Xin Gu [1] and Guozheng Zhang [1]

[1] School of Electrical Engineering, Tiangong University, Tianjin 300387, China; jinxuefeng@tiangong.edu.cn (X.J.); 2031060815@tiangong.edu.cn (S.L.); guxin@tiangong.edu.cn (X.G.); zhangguozheng@tiangong.edu.cn (G.Z.)
[2] WEICHAI Power Co., Ltd., Weifang 261061, China; sunwenb@weichai.com
* Correspondence: chen_wei@tiangong.edu.cn

Abstract: The switching frequency of high-power inverters, such as those used in rail transit traction systems, is low, due to switching loss and heat dissipation limitations. This can result in considerable output voltage harmonics. This paper proposes an optimal SPWM strategy for traction inverters based on non-equally spaced carriers to address this issue. By dividing the fundamental wave cycle into regions according to the principle of three-phase, half-wave, and quarter-wave symmetry, the carrier width is symmetrically changed in each region, and a switching angle sequence is generated by comparing the fundamental wave with the non-isometric carrier. The proposed optimal modulation strategy has lower harmonic content than traditional strategies within a specific modulation range. Enhancing the inverter output waveform leads to increased torque accuracy, lowering additional losses in the motor and avoiding overheating. This results in improved performance, enhanced efficiency, and extended service life of the motor system. To further reduce voltage harmonics across the full-speed range, a multi-mode segmented synchronous modulation strategy is designed based on the optimal modulation strategy for different modulation ranges. Appropriate switching points are selected to improve the stability of the traction drive system across the full-speed range. The effectiveness of the proposed method is verified through simulation and experimental results.

Keywords: SPWM (Sinusoidal Pulse Width Modulation); space vector modulation; inverter; harmonic distortion; carrier ratio

Citation: Jin, X.; Li, S.; Sun, W.; Chen, W.; Gu, X.; Zhang, G. Optimized Synchronous SPWM Modulation Strategy for Traction Inverters Based on Non-Equally Spaced Carriers. *World Electr. Veh. J.* **2023**, *14*, 157. https://doi.org/10.3390/wevj14060157

Academic Editor: Joeri Van Mierlo

Received: 19 May 2023
Revised: 2 June 2023
Accepted: 7 June 2023
Published: 13 June 2023

1. Introduction

With the development of inverter technology, the pulse width modulation strategy is being improved and perfected [1–3]. Rail traction inverters often exhibit low switching frequencies, limited to a few hundred hertz, due to constraints on power device switching losses [4–6]. When the train runs at a low speed, the switching frequency of the high-power traction inverter is relatively high, and the influence of waveform asymmetry is small. Therefore, asynchronous modulation is adopted [7]. When the train runs at medium and high speeds, the switching frequency of the high-power traction inverter is low, and asynchronous modulation may lead to the output voltage waveform of the inverter being asymmetrical and producing significant harmonics. To avoid the harmonics caused by waveform asymmetry, synchronous modulation is adopted [8]. The development of high-performance synchronous modulation strategies has recently become a focal point in rail transit traction inverter research.

There are three primary categories of synchronous modulation strategies: optimization-target-based modulation, space vector modulation (SVPWM), and carrier-based sinusoidal pulse width modulation (SPWM). Optimization-target-based modulation encompasses selective harmonic elimination PWM (SHEPWM) and current harmonic minimization PWM (CHMPWM) [9–12]. While these methods effectively suppress harmonics, their reliance on solving transcendental equations makes them computationally intensive and complex to implement.

SVPWM, on the other hand, achieves output voltage waveform symmetry through volt-second balancing and harmonic optimization by synthesizing reference voltage vectors [13]. Various optimization strategies and principles for synchronous SVPWM modulation have been proposed, as well as methods to improve inverter output performance at high modulation indices [14,15]. Researchers have also explored hybrid modulation approaches that combine different modulation strategies to optimize overall system performance [16–19].

SPWM controls inverter switching device pulse output by comparing fundamental and carrier waveforms. Although this strategy is computationally simple and easy to implement, it results in high harmonic content [20]. Studies have shown that random carrier frequency modulation can effectively reduce harmonic peaks, but the calculations involved are complex and difficult to implement [21–24]. Advances in microcontrollers and FPGAs have, however, facilitated the implementation of SPWM. The researchers proposed an improved SPWM, which can reduce the power loss of THD and inverter by improving the modulation wave shape to improve the bias voltage. Compared with the conventional modulation strategy, it has some advantages at a high switching frequency and modulation index close to 1 [25].

Lastly, synchronous optimal PWM is more suitable for multilevel inverters to find the optimal switching angle to minimize the output harmonic content. This strategy has to give the initial value of the generated angle, which will have a great influence on the modulation strategy. It is also necessary to calculate the optimal value of the angle and determine whether the angle is continuous or not, which leads to a complex calculation and a large number of operations for this type of modulation strategy [26].

In response to the problem of high harmonic content in traditional SPWM, this paper proposes an optimal synchronous SPWM modulation strategy for traction inverters based on non-equally spaced carriers. The SPWM fundamentals, waveform symmetry conditions, and region division are discussed in Section 2. The improved SPWM, waveform evaluation metrics, and simulation validation are discussed in Section 3. Experimental validation is given in Section 4. The proposed PWM modulation method has been proven to be a universal optimization strategy suitable for various motor types, including induction motors, permanent magnet synchronous motors, etc. This optimization effectively reduces the harmonic content in the inverter output, especially at low switching frequencies and carrier ratios, thereby minimizing additional losses of the load motor and improving motor efficiency and system control performance. The effectiveness of this method has been verified by simulation and experimental results.

2. Synchronous SPWM

Basic Principles of Synchronous SPWM

Figure 1 shows the topology of the main circuit of the two-level inverter. By controlling the on/off of power devices, each phase of A, B, and C can output two different switching states. When the base wave is larger than the carrier wave, the high output level is represented by 1; when the base wave is smaller than the carrier wave, the output low level is represented by 0.

In Figure 1, V_{dc} is the DC bus voltage, C is the filter capacitor, S1–S6 is the power device on the three-phase bridge arm of A, B, and C, i_A, i_B, and i_C are the corresponding three-phase AC currents, and M is the motor. To satisfy the symmetry condition, similar to the case of synchronous SVPWM, where the fundamental voltage vector is sectorized in one fundamental cycle, the entire carrier is zoned in synchronous SPWM.

In Figure 2, V_A, V_B, and V_C are the reference voltage fundamental, and one fundamental period of phase A is divided into six regions. In contrast, the control pulses generated by comparing the three-phase fundamental period with the carrier wave are given. To facilitate the observation of the carrier waveform of each region, take phase A as an example to introduce the carrier waveform with the carrier wave peak point over 90°. Phase B and C are the same. The horizontal axis represents the angle, and the vertical axis represents the three-phase voltage amplitude. The dotted line in the middle of area I is a 90° dotted line, and the base point θ_1 Set at 90°.

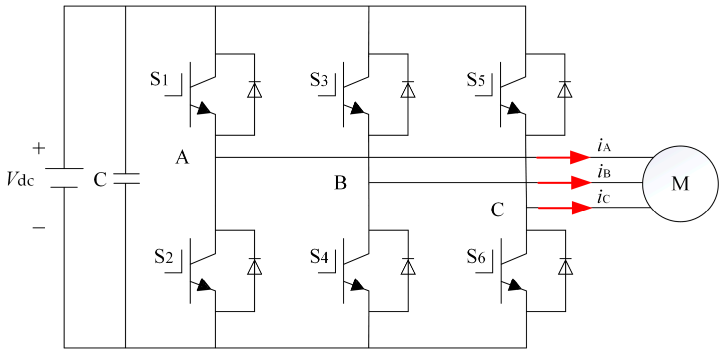

Figure 1. Main circuit topology of a three-phase inverter.

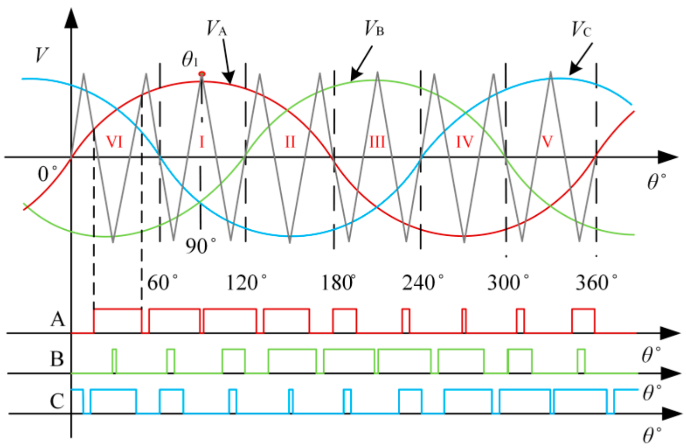

Figure 2. Schematic diagram of synchronous SPWM modulation.

The modulation wave of phase A is represented by the red sine wave, and its corresponding voltage waveform is represented by the red pulse waveform. Likewise, the green sine wave represents the modulation wave of phase B, and the green pulse waveform represents the voltage waveform of phase B. Finally, the blue sine wave represents the modulation wave of phase C, and the blue pulse waveform represents the voltage waveform of phase C. The carrier waveforms in regions I, III, and V are consistent with satisfying the three-phase symmetry principle. Similarly, the carrier waveforms corresponding to regions II, IV, and VI are consistent.

To satisfy the half-wave symmetry principle, the carrier waveforms corresponding to regions I and IV, regions II and III, and regions V and VI should meet odd symmetry.

To satisfy the quarter-cycle symmetry principle, the carriers of the region I have to maintain left-right symmetry with the base point θ_1, i.e., have to meet even symmetry. To keep the carrier wave evenly symmetric at both sides of the base point θ_1, the carrier wave must be peak or trough at the 90° moment.

Based on satisfying the above symmetry principle, to ensure that the carrier does not jump at the boundary, the two boundaries of region I must correspond to the midpoints of the diagonal edges of the carrier. The following design rules can be obtained from the above analysis:

1. The angle of each region is 60°.
2. The carrier waveform in each adjacent region maintains odd symmetry centered on the boundary.

3. The carrier waveform centered on the centerline maintains even symmetry in each region.

The analysis can continue to narrow region I. Because the 90° dashed line is uniformly symmetrical on the left and right sides of the carrier waveform, region I is bounded by 90° in the first 30° of the carrier waveform (60° to 90°), and the carrier waveform can be designed for the whole cycle, so the 30° principle is defined.

A clamping strategy is derived from reducing the harmonic content on the synchronous SVPWM. By analogy, synchronous SPWM can also be 30° clamped and 60° clamped.

3. Optimal Synchronous SPWM for Unequally Spaced Carriers

The optimized synchronous SPWM based on non-equally spaced carriers also has to satisfy the symmetry principle of carrier waveform mentioned above. Based on satisfying the symmetry principle, the carrier waveform of the optimized synchronous SPWM is obtained by the normative design of the carrier waveform. Finally, it is compared with the conventional synchronous SPWM to verify the superiority of the proposed strategy in this paper.

3.1. Optimized Synchronous SPWM Carrier Waveform Design Principles for Non-Equally Spaced Carriers

This paper changes the isometric carrier waveform to a non-isometric carrier waveform. To give a clear explanation of the non-isometric carrier waveform, this paper details two carriers with a two-fold width ratio relationship between them, as defined below:

Conventional synchronous SPWM has the width of each carrier equally spaced and continuous within one fundamental period. The width of the carrier of the optimized synchronous SPWM is non-equally spaced within one cycle.

The carrier waveform diagram for region I is shown in Figure 3. The optimal synchronous SPWM is specified as having two carrier widths in one cycle with a width ratio of two times while keeping the switching frequency constant. According to the design rules, the carrier waveform can be designed under the 30° principle (60° to 90°) to obtain the carrier waveform for the whole cycle.

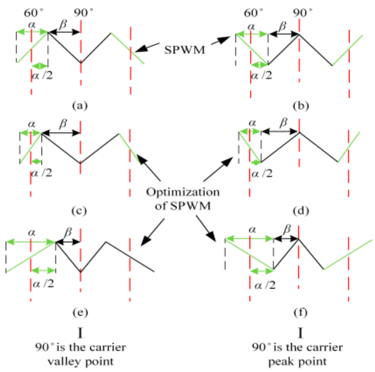

Figure 3. Region 1 Carrier waveform diagram.

As shown in Figure 3, the half-wave widths of the two carriers are respectively α and β. The wide carrier is far away from base point θ_1 and occupies an angle of $\alpha/2$ at 30°. The carrier wave of another width is close to the base point θ_1 and occupies an angle of β at 30° The angle between two adjacent red lines in the region I is 30°, and under the 30° principle, the angle occupied by 30° is taken as γ. γ is expressed as

$$\gamma = \frac{\alpha}{2} + \beta \tag{1}$$

When the width ratio is defined as α rather than β, K_1 and K_2 represent the half wave of two carrier widths, respectively and the number of α and β in the 30° range is:

$$\begin{cases} K_1 = n + 1/2 \\ K_2 = m \end{cases} \tag{2}$$

where n and m are non-negative integers; when n = 0 and m = 1, the carrier waveforms of different modulation strategies are shown in Figure 3. Of course, n and m cannot be infinitely large under a low carrier ratio, and the range of values needs to be determined according to the carrier ratio.

The conventional synchronous SPWM region I carrier waveform is shown as α: β = 1:1 in Figure 3a,b, and the others are optimized synchronous SPWM region I carrier waveforms. Since the magnitude of each carrier width is distributed differently in the region I according to the rule, this optimized synchronous SPWM can be divided into two cases.

The first case is shown in Figure 3c,d α: β = 1:2. The carrier width is not fixed in one cycle, and to maintain symmetry, the region I boundary must be the midpoint of the carrier ramp. The carrier waveform in the figure will make the middle of the region a wider carrier and the two sides of the region a narrower carrier.

The second case is shown in Figure 3e,f α: β = 2:1. The carrier width is not fixed in one cycle. To maintain symmetry, the region I boundary must be the midpoint of the carrier ramp. The carrier waveform in the figure will make the middle of the region a narrower carrier, and the two sides of the region a wider carrier.

3.2. V_{WTHD} for Different Modulation Strategies

Different modulation strategies require consistent evaluation metrics to objectively evaluate their performance. For traction inverters with equal output line voltage magnitude, the value of line voltage weighted total harmonic distortion rate (V_{WTHD}) is usually used as the inverter output waveform quality measure to compare the advantages and disadvantages of different modulation strategies. The definition is as follows:

$$V_{WTHD} = \frac{1}{V_1}\sqrt{\sum\left(\frac{V_n}{n}\right)^2 \ldots (n \neq 1)} \tag{3}$$

where V_1 and V_n are the effective values of the fundamental and sub-harmonic voltage of the line voltage waveform, respectively; therefore, whichever modulation strategy has a low line voltage weighted total harmonic distortion coefficient (V_{WTHD}) displays good performance.

From the definition of modulation strategies in the previous section, three variables exist for performance comparison: carrier ratio (5 to 15), modulation index (0 to 1), and width ratio (α: β). With constant carrier ratio and modulation index but different width ratios, the line voltage weighted total harmonic distortion coefficients of the different modulation strategies are compared by calculation. Figure 4 shows the harmonic content of the conventional and optimized synchronous SPWM for different width ratios when the carrier ratio N = 5, modulation index M = 0.8, K_1 = 0.5, and K_2 = 1, where the width ratio 1:1 is the conventional strategy.

The values of the total harmonic distortion rate of the line voltage with weighting under respective carrier width ratios are represented by the square and circular symbols, when n is a positive integer. As shown in Figure 4, by calculating the harmonic content at different width ratios, it can be seen that the harmonic content in the optimized strategy is lower than that in the conventional strategy, and the harmonic content is lowest when the width ratio is 3:1. Therefore, it can be verified that the optimized strategy has better inverter output performance with lower harmonic content for a specific width ratio.

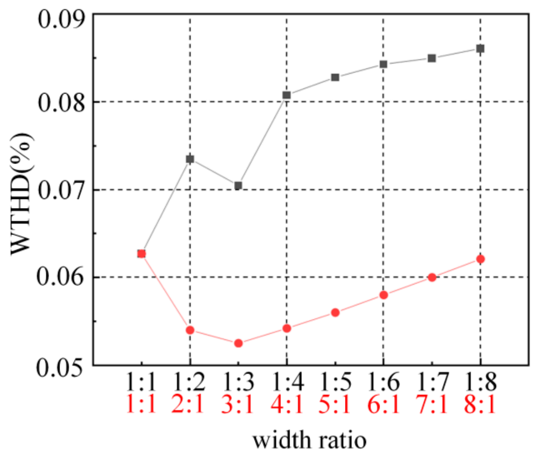

Figure 4. When $N = 5$, $M = 0.8$ and $K_1 = 0$, $K_2 = 1$, different modulation strategies V_{WTHD}.

To further demonstrate the superiority of the strategy proposed in this paper, the conventional synchronous SPWM with a width ratio of 1:1 and the optimized synchronous SPWM with a width ratio of 1:2 and a width ratio of 2:1 are compared, by varying the modulation index and carrier ratio while keeping the width ratio constant. It is verified that the proposed optimized strategy has good harmonic characteristics compared with the conventional strategy over the whole modulation range.

In Figure 4, the switching angle sequence formed under different width ratios is different. According to the switching angle sequence, the value of the voltage weighted total harmonic distortion rate of the output line of the inverter is obtained by Fourier transform. As can be seen from the figure, when the width ratio is 1:3, the optimal switching sngle sequence is formed, resulting in the lowest harmonic content.

The traditional synchronous SPWM width ratio 1:1 is defined as 1–1, the optimized synchronous SPWM width ratio 1:2 is defined as 1–2, and the width ratio 2:1 is defined as 2–1. However, the width ratio 1–2 is a peak or valley point at 90°. The clamp-type and the values of K_1 and K_2 will lead to different strategies. To distinguish strategies more clearly, the following provisions are made:

1. In each cycle, the carrier wave at the 90° position is noted as H if it is a peak and L if it is a trough.
2. Depending on the clamp type, 60° clamp, and 30° clamp are recorded as S and T.

For example, the width ratio 1:2 at 90° is the peak point, and the clamp type is 60° clamp, which is recorded as HS_{1-2}; the same for other strategies. Table 1 shows all modulation strategies with different carrier ratios and width ratios 1–1, 1–2, and 2–1.

Table 1. All modulation strategies with width ratios of 1–1, 1–2, and 2–1 under different carrier ratios.

N	K_1, K_2	Modulation Strategy
5	$K_1 = 0.5, K_2 = 1$	LT_{1-1}, LT_{1-2}, LT_{2-1}
7	$K_1 = 0.5, K_2 = 1$	HS_{1-1}, HS_{1-2}, HS_{2-1}
9	$K_1 = 0.5, K_2 = 1$	H_{1-1}, L_{1-1}, LS_{1-1}, HT_{1-1}, H_{1-2}, L_{1-2}, LS_{1-2}, HT_{1-2}, H_{2-1}, L_{2-1}, LS_{2-1}, HT_{2-1}
11	$K_1 = 0.5, K_2 = 2$	LS_{1-1}, HT_{1-1}, LT_{1-1}, LS_{1-2}, HT_{1-2}, LT_{1-2}, LS_{2-1}, HT_{2-1}, LT_{2-1}
	$K_1 = 1.5, K_2 = 1$	LS_{1-2}, HT_{1-2}, LT_{1-2}, LS_{2-1}, HT_{2-1}, LT_{2-1}
13	$K_1 = 0.5, K_2 = 2$	HS_{1-1}, HS_{1-2}, HS_{2-1}
	$K_1 = 1.5, K_2 = 1$	HS_{1-2}, HS_{2-1}
15	$K_1 = 0.5, K_2 = 2$	H_{1-1}, L_{1-1}, H_{1-2}, L_{1-2}, H_{2-1}, L_{2-1}
	$K_1 = 1.5, K_2 = 1$	H_{1-2}, L_{1-2}, H_{2-1}, L_{2-1}

The characteristic curve of V_{WTHD} when $N = 5$ is shown in Figure 5. When $0 \le M \le 1$, the chosen modulation strategy is $K_1 = 0.5$, $K_2 = 1$ (LT_{2-1}).

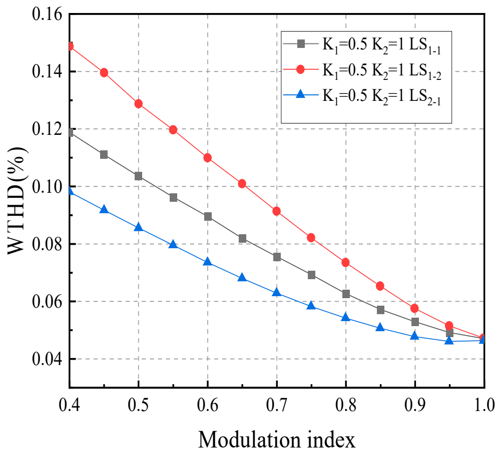

Figure 5. V_{WTHD} corresponding to $N = 5$.

The characteristic curve of V_{WTHD} when $N = 7$ is shown in Figure 6. When $0 \leq M \leq 0.55$, the chosen modulation strategy is $K_1 = 0.5$, $K_2 = 1$ ($HS_{2\text{–}1}$). When $0.55 \leq M \leq 0.82$, the chosen modulation strategy is $K_1 = 0.5$, $K_2 = 1$ ($HS_{1\text{–}1}$).When $0.82 \leq M \leq 1$, the modulation strategy selected is $K_1 = 0.5$, $K_2 = 1$ ($HS_{1\text{–}2}$).

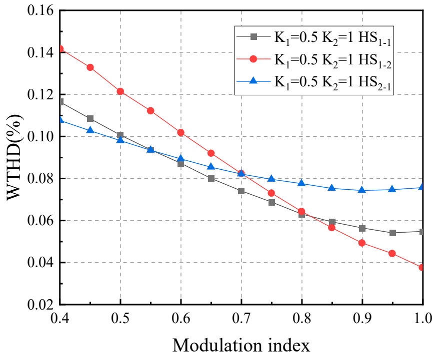

Figure 6. V_{WTHD} corresponding to $N = 7$.

The characteristic curve of V_{WTHD} when $N = 9$ is shown in Figure 7. When $0 \leq M \leq 0.7$, the chosen modulation strategy is $K_1 = 0.5$, $K_2 = 1$ ($L_{1\text{–}1}$). When $0.7 \leq M \leq 1$, the modulation strategy selected is $K_1 = 0.5$, $K_2 = 1$ ($H_{1\text{–}2}$). When the width ratio of the two carriers is fixed, the output harmonic content of the inverter can be changed by changing the modulation index. Normally, the output harmonic content of the inverter decreases with the increase of the modulation index. However, this relationship is not necessarily the case in some modulation index ranges, because the output harmonic content of the inverter is calculated by the value of the line voltage-weighted total harmonic distortion. Therefore, the green line in Figure 7 shows an upward trend at the modulation index of 0.65 to 0.75.

The characteristic curve of V_{WTHD} when $N = 11$ is shown in Figure 8. When $0 \leq M \leq 0.9$, the chosen modulation strategy is $K_1 = 0.5$, $K_2 = 2$ ($HT_{2\text{–}1}$). When $0.9 \leq M \leq 1$, the modulation strategy selected is $K_1 = 0.5$, $K_2 = 2$ ($LT_{1\text{–}2}$).

The characteristic curve of V_{WTHD} when $N = 13$ is shown in Figure 9. When $0 \leq M \leq 0.85$, the chosen modulation strategy is $K_1 = 0.5$, $K_2 = 2$ ($HS_{2\text{–}1}$). When $0.85 \leq M \leq 1$, the modulation strategy selected is $K_1 = 0.5$, $K_2 = 2$ ($HS_{1\text{–}1}$).

The characteristic curve of V_{WTHD} when $N = 15$ is shown in Figure 10. When $0 \leq M \leq 0.65$, the chosen modulation strategy is $K_1 = 0.5$, $K_2 = 2$ ($L_{1\text{–}1}$). When $0.65 \leq M \leq 1$, the modulation strategy selected is $K_1 = 0.5$, $K_2 = 2$ ($L_{1\text{–}2}$).

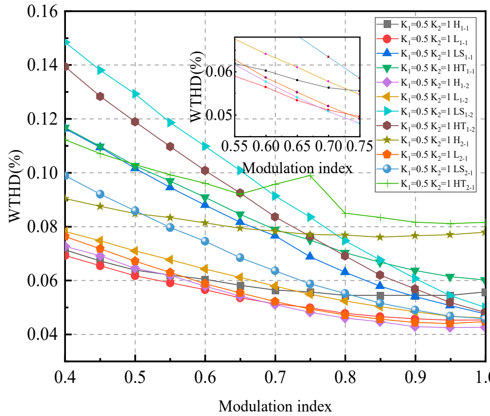

Figure 7. V_{WTHD} corresponding to $N = 9$.

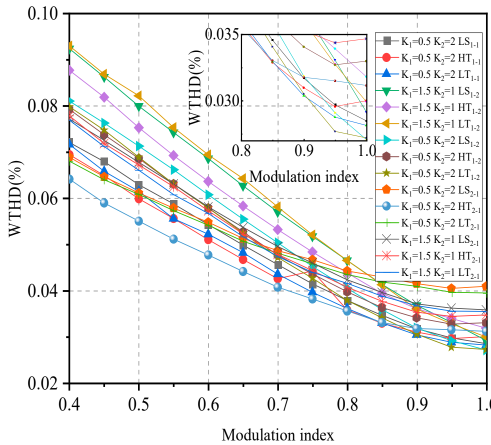

Figure 8. V_{WTHD} corresponding to $N = 11$.

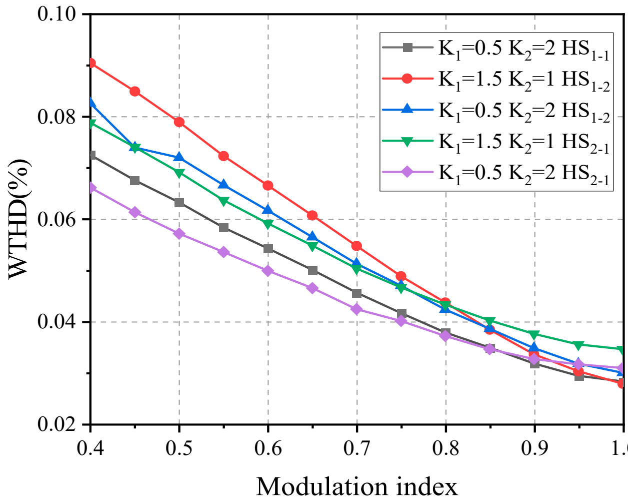

Figure 9. V_{WTHD} corresponding to $N = 13$.

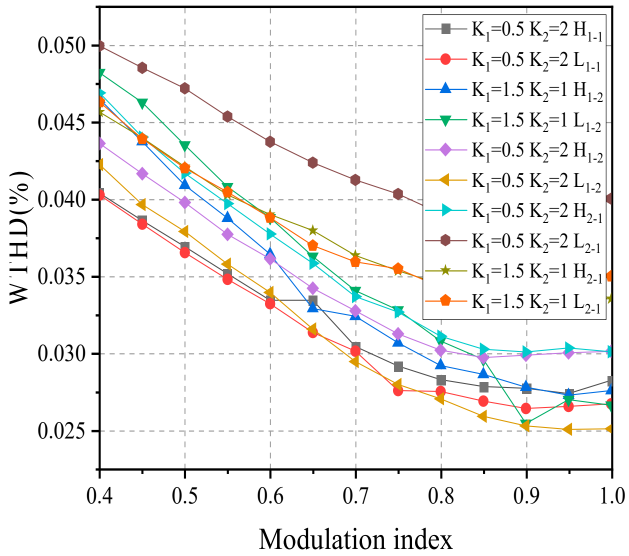

Figure 10. V_{WTHD} corresponding to N = 15.

3.3. Multi-Mode Segmented Synchronous Modulation Strategy

In Figure 11, a plot of the inverter switching frequency variation with fundamental frequency versus modulation index is shown, displaying the effect of multi-mode segmented synchronous modulation. In Figure 11, the modulation index at the low switching frequency is proportional to the fundamental frequency. When the fundamental frequency is low, the effect of waveform asymmetry is less, so asynchronous modulation is used. With the increase of fundamental frequency, the carrier ratio decreases gradually, and the influence of waveform asymmetry is serious. In this case, synchronous modulation is used.

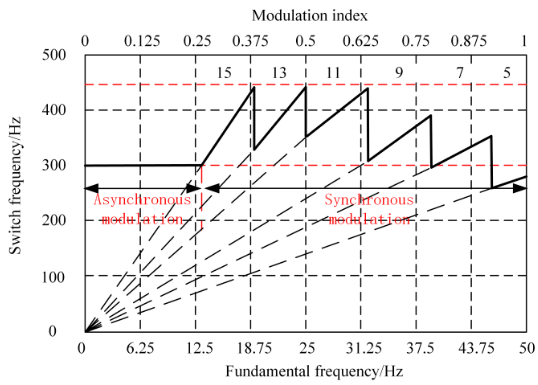

Figure 11. Variation curve of inverter switching frequency with fundamental frequency and modulation index.

The optimal modulation strategy is selected according to the correspondence between the output fundamental frequency of the inverter and the modulation index. The optimal modulation strategy is selected for multi-mode modulation by comparing V_{WTHD} in the whole modulation range according to the comparison principle in Section 3.2. Table 2 shows the optimal modulation strategy patterns under different carrier ratios.

As shown in Figure 11, when the modulation range is 0.64to0.9 and N = 7, the optimal modulation strategy is divided into two types. One is the conventional synchronous SPWM with a modulation range of 0.64 to 0.85, and the other is the optimized synchronous SPWM with a modulation range of 0.85 to 0.9. In the modulation range of 0.85 to 0.9, the two strategies do not differ much. To avoid too many switching times at the same carrier ratio, the conventional synchronous SPWM is used when N = 7. The optimal modulation strategies in Table 2 can be used for multi-mode modulation strategies.

Table 2. Optimal modulation strategy under different carrier ratios.

N	K_1, K_2	Optimal Modulation Strategy
5	$K_1 = 0.5$, $K_2 = 1$	LT_{2-1}
7	$K_1 = 0.5$, $K_2 = 1$	HS_{1-1}
9	$K_1 = 0.5$, $K_2 = 1$	L_{1-1}
11	$K_1 = 0.5$, $K_2 = 2$	HT_{2-1}
13	$K_1 = 0.5$, $K_2 = 2$	HS_{2-1}
15	$K_1 = 0.5$, $K_2 = 2$	L_{1-1}

4. Experimental Results and Analysis

In this paper, to verify the superiority of the proposed optimized synchronous SPWM based on non-equally spaced carriers compared with the conventional synchronous SPWM and the feasibility of the improved hybrid multi-mode synchronous modulation strategy, the OP5700, a rapid prototyping system from Opal Real-time Technologies LTD., Canada is used as the control circuit. An experiment is conducted using a two-level inverter with three imperix PEB8024 half-bridge modules, manufactured in Switzerland, connected in parallel. The experimental system is shown in Figure 12.

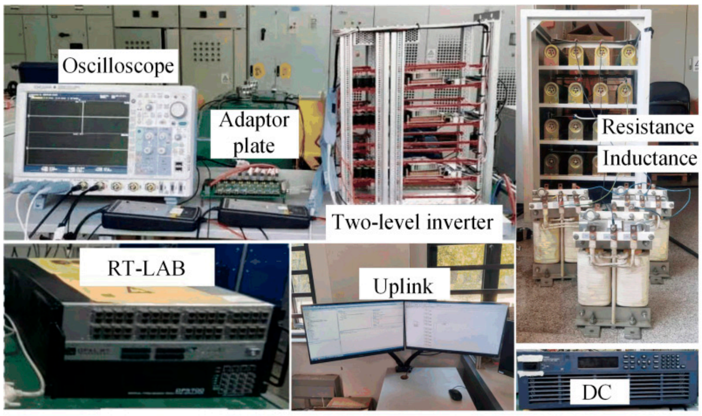

Figure 12. Experimental platform.

With the above experimental system, the conventional synchronous SPWM in different carrier ratios is experimentally compared with the optimized synchronous SPWM with non-equally spaced carriers proposed in this paper. The experimental system parameters are shown in Table 3.

Table 3. Parameters of the system.

Parameter	Values	Unit
DC-side capacitance/C	780	µF
DC-link voltage/V_{dc}	150	V
Load resistance/R	10	Ω
Load inductance/L	20	mH
Fundamental frequency/f	50	Hz
Dead-time/t	600	ns

ns is the unit of time.

When the carrier ratio $N = 7$ and the modulation index $M = 0.8$, the harmonic content of the conventional synchronous modulation strategy is lower compared with the optimized synchronous SPWM with non-equally spaced carriers. Therefore, when the carrier ratio $N = 7$ and the modulation index $M = 0.8$, the conventional synchronous modulation strategy is better, so the comparison is not performed in the experiment.

Since the inverter output current is related to the system losses and other factors, the total harmonic distortion rate of current (I_{THD}) is used as the evaluation index for evaluating the PWM output waveform in the data processing:

$$I_{THD} = \frac{1}{I_1}\sqrt{\sum (I_n)^2 \ldots}(n \geq 1) \tag{4}$$

where I_1 and I_n are the RMS values of the fundamental and sub-harmonic currents of the current waveform, respectively. Voltage and current signals are collected by the voltage and current probe and displayed on the oscilloscope, and then stored in the oscilloscope and input to the upper computer through the u disk. The sampled signal is processed by sampling and filtering circuits. Yokogawa brand voltage and current probe and oscilloscope are used in the experiment.

In Figures 13–17, the waveforms of the inverter AB-phase output line voltage (V_{AB}) and A-phase phase current (i_A) are compared for different carrier ratios (5, 9, 11, 13, 15) and modulation index M = 0.8 under the optimal strategy in the conventional synchronous SPWM and the optimal strategy in the optimized synchronous SPWM.

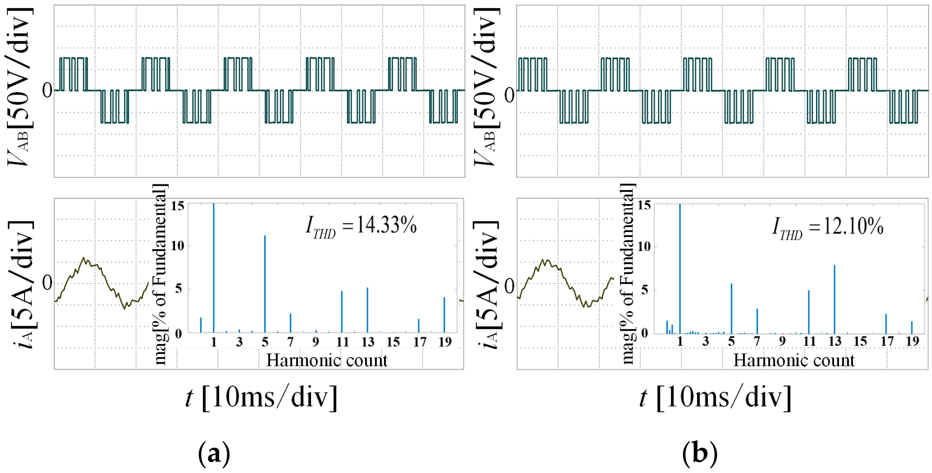

Figure 13. Line voltage waveform and phase current waveform at carrier wave ratio 5: (**a**) traditional synchronous SPWM (LS_{2-1}); (**b**) optimized synchronous SPWM (LT_{2-1}).

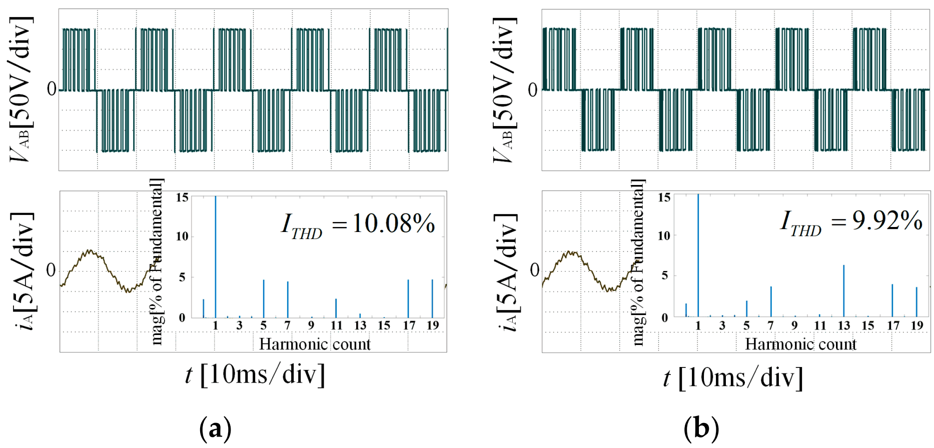

Figure 14. Line voltage waveform and phase current waveform at carrier wave ratio 9: (**a**) traditional synchronous SPWM (L_{1-1}); (**b**) optimized synchronous SPWM (H_{1-2}).

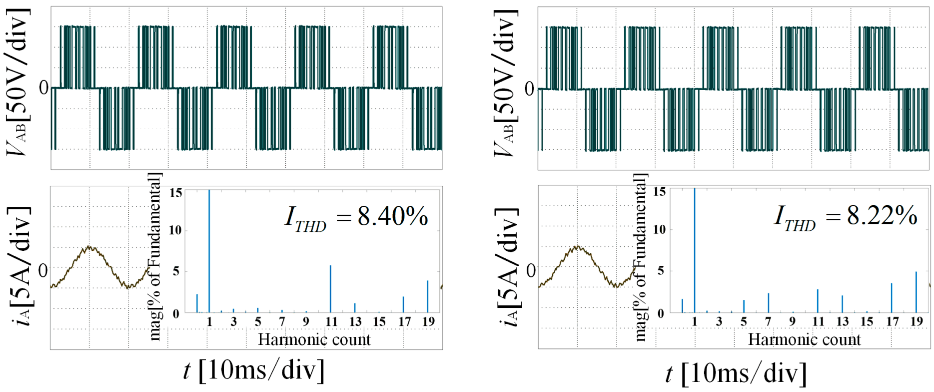

(**a**) (**b**)

Figure 15. Line voltage waveform and phase current waveform at carrier wave ratio 11: (**a**) traditional synchronous SPWM ($HT_{1\text{–}1}$); (**b**) optimized synchronous SPWM ($HT_{2\text{–}1}$).

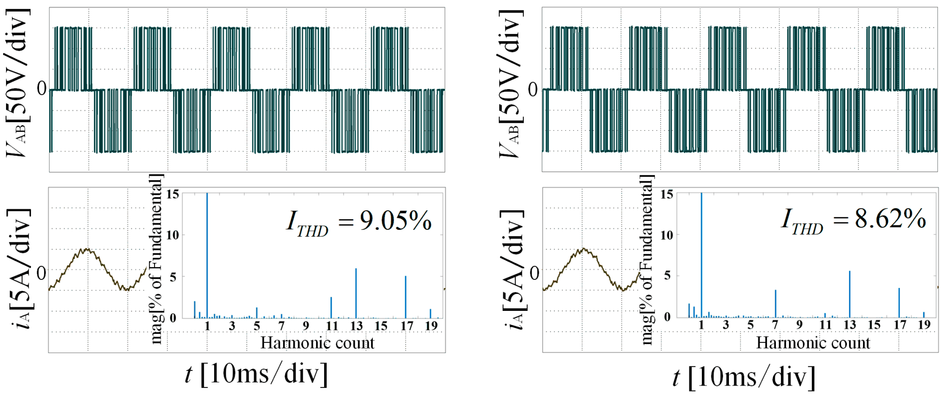

(**a**) (**b**)

Figure 16. Line voltage waveform and phase current waveform at carrier wave ratio 13: (**a**) traditional synchronous SPWM ($HS_{1\text{–}1}$); (**b**) optimized synchronous SPWM ($HS_{2\text{–}1}$).

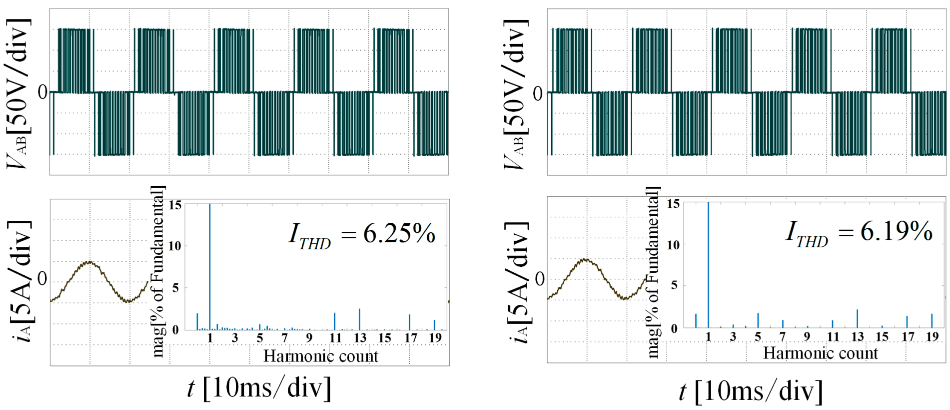

(**a**) (**b**)

Figure 17. Line voltage waveform and phase current waveform at carrier wave ratio 15: (**a**) traditional synchronous SPWM ($L_{1\text{–}1}$); (**b**) optimized synchronous SPWM ($L_{1\text{–}2}$).

As shown in Figure 13, when the modulation index is M = 0.8, the traditional synchronous SPWM ($LS_{2\text{–}1}$) I_{THD} = 14.33%, and the optimized synchronous SPWM ($LT_{2\text{–}1}$) I_{THD} = 12.10% with K_1 = 0.5 and K_2 = 1.

As shown in Figure 14, when the modulation index is M = 0.8, the traditional synchronous SPWM (L_{1-1}) I_{THD} = 10.08%, and the optimized synchronous SPWM (H_{1-2}) I_{THD} = 9.92% with K_1 = 0.5 and K_2 = 1.

As shown in Figure 15, when the modulation index is M = 0.8, the traditional synchronous SPWM (HT_{1-1}) I_{THD} = 8.40%, and the optimized synchronous SPWM (HT_{2-1}) I_{THD} = 8.22% with K_1 = 0.5 and K_2 = 2.

As shown in Figure 16, when the modulation index is M = 0.8, the traditional synchronous SPWM (HS_{1-1}) I_{THD} = 9.05%, and the optimized synchronous SPWM (HS_{2-1}) I_{THD} = 8.62% with K_1 = 0.5 and K_2 = 2.

As shown in Figure 17, when the modulation index is M = 0.8, the traditional synchronous SPWM (L_{1-1}) I_{THD} = 6.25%, and the optimized synchronous SPWM (L_{1-2}) I_{THD} = 6.19% with K_1 = 0.5 and K_2 = 2.

In this study, we use M = 0.8 for experimental verification. When M = 0.8, the proposed optimization strategy with different carrier ratios does not necessarily have a significantly better harmonic suppression effect than the corresponding traditional strategy; in some cases, the optimization strategy may only be slightly better. This is because the proposed optimization strategy will be optimal compared to the traditional strategy at different M values for various carrier ratios. Using N = 5 as an example, the lower the M, the better the harmonic suppression effect of the optimization strategy.

Additionally, as the carrier ratio decreases, the fewer pulses there are in the fundamental cycle and the greater the difference between the switching sequences formed by the proposed optimized strategy and those formed by the conventional strategy. The experimental results for the carrier ratio of 5 demonstrate that the optimized strategy has a significant harmonic suppression effect compared to the conventional strategy.

Conversely, as the number of pulses in the fundamental cycle increases with the carrier ratio, the difference between the switching sequences formed by the proposed optimized strategy and those formed by the conventional strategy becomes less significant. This results in the optimized strategy having a harmonic suppression effect compared to the conventional strategy, but it is not substantial. The purpose of using M = 0.8 for comparison is to facilitate the execution of the experiment.

The experiments indicate that when the modulation index M = 0.8, the total harmonic distortion rate of the inverter output current under the effect of the optimization strategy proposed in this paper is lower than that of the conventional strategy, and the quality of the inverter output waveform is better, verifying the superiority of the optimization strategy.

As shown in Figure 18, to achieve smooth switching and avoid current inrush problems, it is necessary to ensure that under different carrier ratios, the six power devices of the three phases before and after switching have no simultaneous switching action, and the power devices of each phase cannot be turned on and off at the same time. Phase A, phase B, and phase C switching points are staggered by $2\pi/3$ for switching.

The switching points selected in this paper are all chosen near the peak and valley points of the carrier at the switching frequency. As shown in Figure 18, switching at the peak and valley points of the carrier can effectively eliminate current spikes and significantly decrease voltage harmonic content across the entire speed range, thus enhancing the output voltage quality of the inverter.

Compared to traditional SPWM, this optimization approach improves the waveform quality of the inverter output, increases torque accuracy, and decreases motor losses, thereby enhancing the operating efficiency of the traction drive system. Additionally, the high-quality inverter output waveform improves torque accuracy, thereby boosting system performance.

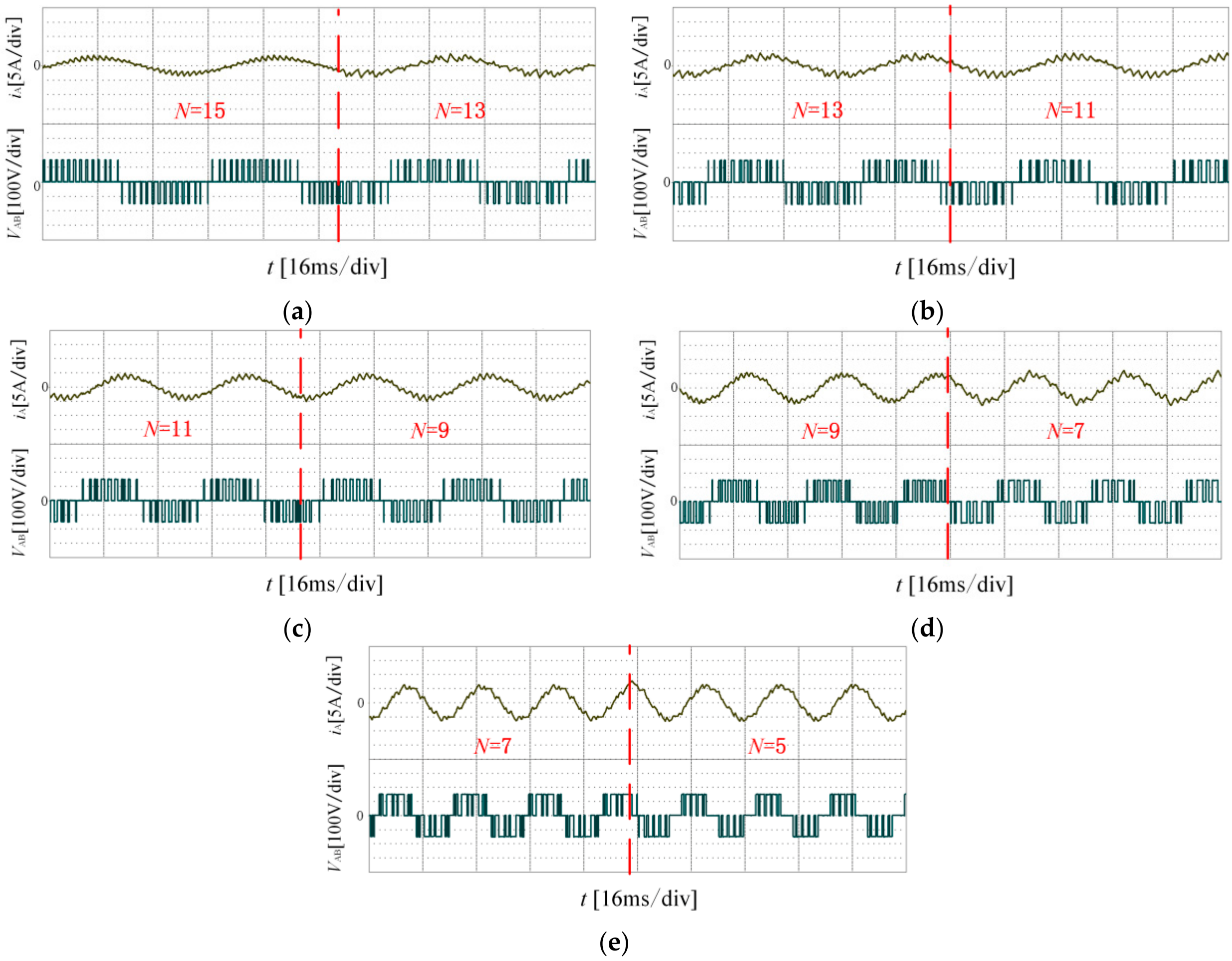

Figure 18. Smooth switching between adjacent different carrier ratios: (**a**) carrier ratio 15 to 13; (**b**) carrier ratio 13 to 11; (**c**) carrier ratio 11 to 9; (**d**) carrier ratio 9 to 7; (**e**) carrier ratio 7 to 5.

5. Conclusions

Employing a modified version of SPWM for the control of inverters reduces the harmonic content of the generated waveforms. Comparing the improved strategy with the traditional strategy, it can be seen that the optimized strategy can produce better inverter output waveform quality in a specific modulation index range. It is capable of operating at very low switching frequencies. This reduces the switching loss of the inverter.

In addition, a multi-mode segmented synchronous modulation strategy is proposed to reduce the voltage harmonics of each frequency band in the whole velocity domain by appropriate switching points. This improves the inverter output voltage quality.

The effectiveness of the proposed optimized synchronous SPWM based on non-equidistant carriers is verified by experiments. The stability of the traction transmission system is improved by adopting multi-mode segmented synchronous modulation based on an optimization strategy. The optimization strategy, based on non-equidistant carriers, is an effective solution to improve the performance of traction inverters.

Limitations of optimization strategy: in this paper, a non-equally spaced carrier is used to reduce V_{WTHD}. However, in practical application, the design of non-equally spaced carriers is more complex than that of traditional equally spaced carriers.

In this paper, the improved modulation strategy is verified by a resistive load experiment. Future research will proceed with the following goals:

1. Applying the strategy to the closed-loop control of the motor system.
2. Combining the modulation algorithm and advanced control strategy proposed in this paper.

Author Contributions: Conceptualization, X.J.; data curation, S.L.; funding acquisition, W.C.; investigation, X.G. and G.Z.; methodology, X.J.; project administration, W.S. and W.C.; supervision, W.C.; validation, X.G.; writing—original draft, S.L.; writing—review and editing, W.C. All authors have read and agreed to the published version of the manuscript.

Funding: This research was funded by the National Natural Science Foundation of China, grant number 52077156; the Key Program of Tianjin Natural Science Foundation, grant number 20JCZDJC00020.

Institutional Review Board Statement: Not applicable.

Informed Consent Statement: Not applicable.

Data Availability Statement: Not applicable.

Conflicts of Interest: The authors declare no conflict of interest. The funders had no role in the design of the study; in the collection, analyses, or interpretation of data; in the writing of the manuscript; or in the decision to publish the results. W.S. is an employee of WEICHAI Power Co., Ltd., Shandong 261061, China. The paper reflects the views of the scientists and not the company.

References

1. Wang, J.; Miao, Q.; Zhou, X.; Sun, L.; Gao, D.; Lu, H. Current Control Method of Vehicle Permanent Magnet Synchronous Motor Based on Active Disturbance Rejection Control. *World Electr. Veh. J.* **2023**, *14*, 2. [CrossRef]
2. Gao, W.; Zhang, G.; Hang, M.; Cheng, S.; Li, P. Sensorless Control Strategy of a Permanent Magnet Synchronous Motor Based on an Improved Sliding Mode Observer. *World Electr. Veh. J.* **2021**, *12*, 74. [CrossRef]
3. Kang, J.-W.; Hyun, S.-W.; Kan, Y.; Lee, H.; Lee, J.-H. A Novel Zero Dead-Time PWM Method to Improve the Current Distortion of a Three-Level NPC Inverter. *Electronics* **2020**, *9*, 2195. [CrossRef]
4. Vijayakumar, A.; Stonier, A.A.; Peter, G.; Loganathan, A.K.; Ganji, V. Power quality enhancement in asymmetrical cascaded multilevel inverter using modified carrier level shifted pulse width modulation approach. *IET Power Electron.* **2022**, 1–13. [CrossRef]
5. Xu, W.; Chan, C.H.; Chan, K.W.; Wing, S.; Ho, S.L.; Liu, M. A quantitative harmonics analysis approach for sinusoidal pulse-width-modulation based Z-source inverters. *IET Power Electron.* **2022**, *15*, 815–824. [CrossRef]
6. Liu, J.; Zhang, W.; Xiao, F.; Lian, C.; Gao, S. Six-step mode control of IPMSM for railway vehicle traction eliminating the DC offset in input current. *IEEE Trans. Power Electron.* **2019**, *34*, 8981–8993. [CrossRef]
7. Suhel, S.M.; Maurya, R. A new switching sequences of SVPWM for six-phase induction motor with features of reduced switching losses. *CES Trans. Electr. Mach. Syst.* **2021**, *5*, 100–107. [CrossRef]
8. Yang, Y.-P.; Peng, M.-T. A Surface-Mounted Permanent-Magnet Motor with Sinusoidal Pulsewidth-Modulation-Shaped Magnets. *IEEE Trans. Magn.* **2019**, *55*, 2873773. [CrossRef]
9. Siddique, M.D.; Mekhilef, S.; Padmanaban, S.; Memon, M.A.; Kumar, C. Single-Phase Step-Up Switched-Capacitor-Based Multilevel Inverter Topology with SHEPWM. *IEEE Trans. Ind. Appl.* **2021**, *57*, 3107–3119. [CrossRef]
10. Li, Y.; Zhang, X.-P.; Li, N. An Improved Hybrid PSO-TS Algorithm for Solving Nonlinear Equations of SHEPWM in Multilevel Inverter. *IEEE Access* **2022**, *10*, 48112–48125. [CrossRef]
11. Guan, B.; Doki, S. A Current Harmonic Minimum PWM for Three-Level Converters Aiming at the Low-Frequency Fluctuation Minimum of Neutral-Point Potential. *IEEE Trans. Ind. Electron.* **2019**, *66*, 3380–3390. [CrossRef]
12. Zhang, Z.; Ge, X.; Tian, Z.; Zhang, X.; Tang, Q.; Feng, X. A PWM for Minimum Current Harmonic Distortion in Metro Traction PMSM with Saliency Ratio and Load Angle Constrains. *IEEE Trans. Power Electron.* **2018**, *33*, 4498–4511. [CrossRef]
13. Diao, N.; Sun, X.; Song, C.; Zhang, Q.; Zhang, Z. A Multimodulation Times SVPWM for Dead-Time Effect Elimination in Three-Level Neutral Point Clamped Converters. *IEEE Trans. Ind. Electron.* **2021**, *68*, 5476–5485. [CrossRef]
14. Yan, Q.; Zhang, X.; Zhao, T.; Yuan, X.; Zhao, R. An Analytical Simplified Three-Level SVPWM with Unified Zero-Sequence Component Injection. *IEEE Trans. Power Deliv.* **2022**, *37*, 2417–2420. [CrossRef]
15. Yan, Q.; Zhou, Z.; Wu, M.; Yuan, X.; Zhao, R.; Xu, H. A Simplified Analytical Algorithm in abc Coordinate for the Three-Level SVPWM. *IEEE Trans. Power Electron.* **2021**, *36*, 3622–3627. [CrossRef]
16. Chen, K.-Y.; Xie, Y.-L. Reducing Harmonics Distortion in Five-Phase VSI Using Space-Vector-Based Optimal Hybrid PWM. *IEEE Trans. Power Electron.* **2017**, *32*, 2098–2113. [CrossRef]
17. Yang, H.; Zhang, Y.; Yuan, G.; Walker, P.D.; Zhang, N. Hybrid Synchronized PWM Schemes for Closed-Loop Current Control of High-Power Motor Drives. *IEEE Trans. Ind. Electron.* **2017**, *64*, 6920–6929. [CrossRef]
18. Qiu, Z.; Huang, X.; Ma, K.; Kong, Z.; Liu, X. Sideband Vibro-Acoustic Responses and Improvements with Different Pulsewidth Modulation Strategies in Permanent Magnet Synchronous Motor for Electric Vehicle. *IEEE J. Emerg. Sel. Top. Power Electron.* **2022**, *10*, 7098–7108. [CrossRef]
19. Zhang, G.; Zhou, Z.; Shi, T.; Xia, C. An Improved Multimode Synchronized Space Vector Modulation Strategy for High-Power Medium-Voltage Three-Level Inverter. *IEEE Trans. Power Electron.* **2021**, *36*, 4686–4696. [CrossRef]

20. Sahoo, S.K.; Bhattacharya, T. Phase-Shifted Carrier-Based Synchronized Sinusoidal PWM Techniques for a Cascaded H-Bridge Multilevel Inverter. *IEEE Trans. Power Electron.* **2018**, *33*, 513–524. [CrossRef]
21. Gamoudi, R.; Chariag, D.E.; Sbita, L. A review of spread-spectrum -based PWM technique—A novel fast digital implementation. *IEEE Trans. Power Electron.* **2018**, *33*, 10292–10307. [CrossRef]
22. Drissi, K.E.K.; Luk, P.C.K.; Wang, B.; Fontaine, J. Effects of symmetric distribution laws on spectral power density in randomized PWM. *IEEE Power Electron. Lett.* **2003**, *1*, 41–44. [CrossRef]
23. Xu, J.; Nie, Z.; Zhu, J. Characterization and Selection of Probability Statistical Parameters in Random Slope PWM Based on Uniform Distribution. *IEEE Transs. Power Electron.* **2021**, *36*, 1184–1192. [CrossRef]
24. Huang, Y.; Xu, Y.; Zhang, W.; Zou, J. Hybrid RPWM technique based on modified SVPWM to reduce the PWM acoustic noise. *IEEE Trans. Power Electron.* **2019**, *34*, 5667–5674. [CrossRef]
25. Biswas, S.P.; Anower, M.S.; Sheikh, M.R.I.; Islam, M.R.; Kouzani, A.Z.; Mahmud, M.P. A New Modulation Technique to Improve the Performance of Three Phase Inverters. In Proceedings of the IEEE International Conference on Applied Superconductivity and Electromagnetic Devices, Tianjin, China, 16–18 October 2020; pp. 1–2.
26. Rathore, A.K.; Holtz, J.; Boller, T. Synchronous Optimal Pulsewidth Modulation for Low-Switching-Frequency Control of Medium-Voltage Multilevel Inverters. *IEEE Trans. Ind. Electron.* **2010**, *57*, 2374–2381. [CrossRef]